A Preliminary Study of Factors Influencing the Stiffness of Aerial Cable Towed Systems

Vincenzo Di Paola, Edoardo Idà, Matteo Zoppi, Stéphane Caro

A Preliminary Study of Factors Influencing the Stiffness of Aerial Cable Towed Systems

Vincenzo Di Paola [1,2], Edoardo Idà [3], Matteo Zoppi [1] and Stéphane Caro [4]

[1] University of Genova - DIME, Genova, Italy vincenzo.dipaola@edu.unige.it, matteo.zoppi@unige.it

[2] École Centrale de Nantes - LS2N, Nantes, France

[3] University of Bologna - DIN, Bologna, Italy edoardo.ida@unibo.it

[4] CNRS, Laboratoire des Sciences du Numérique de Nantes, Nantes, France stephane.caro@ls2n.fr

Abstract There is a growing attraction for robotic aerial systems in the academic world and in industry. Aerial Cable Towed Systems (ACTSs) are naturally subjected to various unknown external actions (wind, human, etc.). Accordingly, it is crucial to characterize their stiffness both for balancing external disturbances and for their design. Thus, in this paper, an ACTS with a point-mass end-effector, subjected to a generic force, is considered. The effect of the number of cables and the cable arrangement on the stiffness of the ACTSs is investigated. It turns out that the cable arrangement is the factor that enhances most the stiffness of the ACTSs.

1 Introduction

The last few decades have witnessed great advances in the domain of aerial robotics. These robots gained attention because of their potential applications. Initially, they were employed for mapping, surveillance and monitoring operations. Subsequently, interest in infrastructure maintenance operations, search-and-rescue (S&R), etc. led scientists to spend effort on the control and design of Aerial Cable Towed Systems (ACTSs) (Villa et al., 2018). Many of the above-mentioned operations involve coping with external forces (i.e. physical interaction) (Tognon and Franchi, 2020). Therefore, the study of the stiffness of these systems plays a central role. Indeed, the ACTSs can take infinite configurations and the strict relationship between the available wrench, the stiffness and their configuration is the reason behind this work. Recently, the first studies concerning the available wrench set to evaluate the robustness of the equilibrium of these robots were conducted in Erskine et al. (2019a). Despite the differences between ACTSs and Cable-Driven Parallel Robots (CDPRs),

the wrench feasibility analysis of ACTS described in Erskine et al. (2019a) was based on the approach introduced in Bouchard et al. (2010) for the wrench feasibility of CDPRs. The importance of the wrench analysis lies in being able to assess the *feasibility* of a task. Hence, the so-called capacity margin was defined in Ruiz et al. (2015). This capacity margin gave rise to a series of contributions in which the ACTS should accomplish a task while re-configuring. The optimal configuration was chosen with respect to the capacity margin (Erskine et al., 2019b) (Ya et al., 2021). So far, presented works assess the task feasibility by considering only the capacity margin (available wrench). However, the cables introduce compliance into the system and the overall stiffness should also be considered for optimal results.
This paper aims to analyze the effect of the cable arrangement, the number of cables and the configuration parameters of the ACTS on its stiffness. The proposed approach focuses on the use of a directional stiffness index to quantify and compare the effects of cable arrangement and number.
The paper is organised as follows. Section 2 recalls the static model of an ACTS. Section 3 provides some definitions of the stiffness and directional stiffness of an ACTS. Section 4 describes the methodology used to evaluate the effect of the cable arrangement and the number of cables on the directional stiffness of an ACTS. Conclusions and future work are drawn in section 5.

2 System modeling

Let's consider a generic ACTS with n cables and a point-mass load as shown in Figure 1. The symbols used to describe its configuration are summarised in Table 1. The static equilibrium for the point-mass load is given by:

$$\mathbf{W}\mathbf{t} + \mathbf{w}_e = \mathbf{0} \tag{1}$$

where $\mathbf{t}$ is the cable tension vector containing each cable tension t_i, $\mathbf{w}_e$ is the external wrench and $\mathbf{W}$ is the so-called wrench matrix, which can be expressed as:

$$\mathbf{W} = \begin{bmatrix} \mathbf{q}_1 & \mathbf{q}_2 & \dots & \mathbf{q}_n \end{bmatrix} \tag{2}$$

3 Stiffness modeling

Based on previous CDPR stiffness modeling (Moradi, 2013) (Behzadipour, 2006), the stiffness of an ACTS can be defined as:

$$\mathbf{K} = -\frac{\delta \mathbf{w}_e}{\delta \mathbf{x}_L} \tag{3}$$

Table 1. Nomenclature.

Symbols	Physical meaning	Symbols	Physical meaning
F_O, F_{Q_i}	inertial and ith drone frames	$\mathbf{q}_i \in \mathbb{R}^3$	unit vector of the ith cable in F_O
O, Q_i	origin of inertial and ith drone frames	$f_i \in \mathbb{R}$	thrust force of the ith drone
$m \in \mathbb{R}$	mass of each drone	$l_i \in \mathbb{R}$	ith cable length
$\mathbf{x}_L \in \mathbb{R}^3$	position of the load in F_O	$g \in \mathbb{R}$	gravity constant

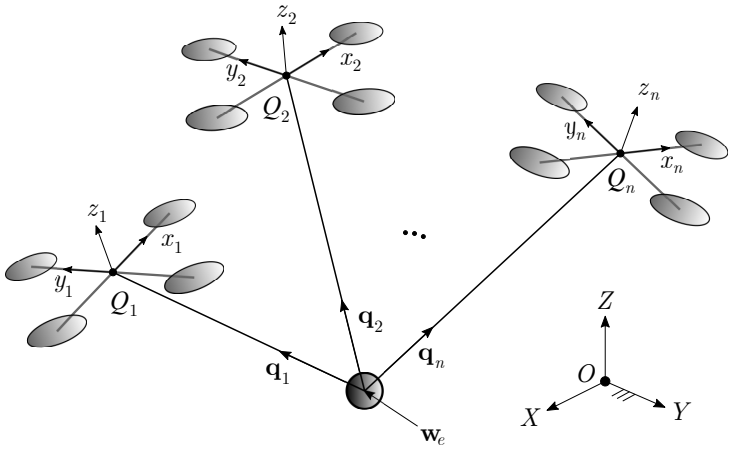

Figure 1. Scheme of a generic ACTS with n cables and a suspended point-mass load.

where a small variation in the external wrench $\delta\mathbf{w}_e$ generates a small displacement of the load $\delta\mathbf{x}_L$. Explicitly, substituting (1) into (3) gives:

$$\mathbf{K} = \frac{\delta}{\delta\mathbf{x}_L}\big(\mathbf{W}\mathbf{t}\big) = \frac{\delta\mathbf{W}}{\delta\mathbf{x}_L}\mathbf{t} + \mathbf{W}\frac{\delta\mathbf{t}}{\delta\mathbf{x}_L} = \frac{\delta\mathbf{W}}{\delta\mathbf{x}_L}\mathbf{t} + \mathbf{W}\frac{\delta\mathbf{t}}{\delta\mathbf{l}}\frac{\delta\mathbf{l}}{\delta\mathbf{x}_L} = \frac{\delta\mathbf{W}}{\delta\mathbf{x}_L}\mathbf{t} + \mathbf{W}\frac{\delta\mathbf{t}}{\delta\mathbf{l}}\mathbf{W}^T \quad (4)$$

where $\mathbf{l} = \begin{bmatrix} l_1 & l_2 & \dots & l_n \end{bmatrix}$. Defining $\frac{\delta\mathbf{t}}{\delta\mathbf{l}} = diag[k_1, k_2, \dots, k_n]$ leads to the so-called *passive stiffness matrix* $\mathbf{K}_p = \mathbf{W}diag[k_1, k_2, \dots, k_n]\mathbf{W}^T = \sum_{i=1}^{n} k_i\mathbf{q}_i\mathbf{q}_i^T$ that is a function of cable arrangement and cable elasticity k_i whereas $\mathbf{K}_a = \frac{\delta\mathbf{W}}{\delta\mathbf{x}_L}\mathbf{t} = \sum_{i=1}^{n} \frac{t_i}{l_i}(\mathbb{I}_3 - \mathbf{q}_i\mathbf{q}_i^T)$ is the *active stiffness matrix* and depends on cable tensions t_i and cable lengths l_i, $i = 1, \dots, n$. Thus, the stiffness matrix $\mathbf{K}$ is:

$$\mathbf{K} = \sum_{i=1}^{n} \frac{t_i}{l_i}(\mathbb{I}_3 - \mathbf{q}_i\mathbf{q}_i^T) + \sum_{i=1}^{n} k_i\mathbf{q}_i\mathbf{q}_i^T = \mathbf{K}_a + \mathbf{K}_p \quad (5)$$

where $\mathbb{I}_3$ is the identity matrix of dimension 3.

Remark 3.1 (Effects of k_i, l_i and t_i on the ACTS stiffness)**.** Equation (5) states that $\mathbf{K}$ is directly proportional to t_i and k_i and inversely proportional to l_i. Therefore, increasing t_i and k_i leads to an increase in $\mathbf{K}$ and vice-versa for l_i. The tension values can not be chosen freely. They must have lower and upper bounds and depend on the ACTS configuration. Cable lengths are practically limited to guarantee quick changes in the cable directions during the operation of the ACTSs. Note that in series with the cable stiffness k_i, the drone also contribute to the stiffness similarly to the winches of the CDPRs. The contribution of the drone stiffness will be the subject of future work.

It is not always necessary to maximize the overall stiffness of a mechanism. For instance, for extinguishing a building fire as described in Jamshidifar and Khajepour (2020), the ACTS should remain almost static in front of the fire while water flows out from the nozzle suspended by the quadrotors and cables. Hence, depending on the task at hand, maximizing the stiffness in one direction may be sufficient. In this perspective, the *directional stiffness index* can be defined as (Moradi, 2013):

$$k_{ds} = \frac{||\mathbf{w}_e||}{||(\mathbf{K}^{-1}\mathbf{w}_e)^T \frac{\mathbf{w}_e}{||\mathbf{w}_e||}||} \tag{6}$$

which evaluates the stiffness along the direction of the external wrench $\mathbf{w}_e$. The solution of equation (1) in terms of tensions can be written in a general form as:

$$\mathbf{t} = -\mathbf{W}^{\dagger}\mathbf{w}_e + \mathbf{N}\boldsymbol{\lambda} \tag{7}$$

where $\mathbf{W}^{\dagger} = \mathbf{W}^T(\mathbf{W}\mathbf{W}^T)^{-1}$ is the pseudo-inverse matrix of $\mathbf{W}$, $\mathbf{N} \in \mathbb{R}^{n\times(n-3)}$ contains the vectors that span the kernel of $\mathbf{W}$ and $\boldsymbol{\lambda} \in \mathbb{R}^{(n-3)}$. Let $\mathfrak{F}$ be the n-dimensional box of feasible tensions:

$$\mathfrak{F} := \{\mathbf{t} \in \mathbb{R}^n \,|\, t_{min,i} \leq t_i \leq t_{max,i},\, i = 1, ..., n\} \tag{8}$$

with tension limits $t_{min,i}$ and $t_{max,i}$ depending on the drone thrust limits f_{min} and f_{max} and their attitude as derived in Erskine et al. (2019a):

$$t_{min,i} = mgq_{z,i} + \sqrt{f_{min}^2 + m^2g^2(q_{z,i}^2 - 1)} \tag{9}$$

$$t_{max,i} = mgq_{z,i} + \sqrt{f_{max}^2 + m^2g^2(q_{z,i}^2 - 1)} \tag{10}$$

Since the feasible tensions belong to a convex set due to the tension limits $t_{min,i}$ and $t_{max,i}$, the lambda space $\mathfrak{L}$ can be defined as:

$$\mathfrak{L} := \{\lambda \in \mathbb{R}^{(n-3)} \,|\, \mathbf{t}_{min} \leq -\mathbf{W}^{\dagger}\mathbf{w}_e + \mathbf{N}\boldsymbol{\lambda} \leq \mathbf{t}_{max}\} \tag{11}$$

which, in turn, is convex. Assume we want to minimize the displacement (i.e. maximize the stiffness) of the load $\delta\mathbf{x}_L = \mathbf{K}^{-1}\delta\mathbf{w}_e$ along the y direction, namely $\delta\mathbf{x}_{L,y}$. Then, the optimal $\boldsymbol{\lambda}$ vector can be obtained by solving the following optimization problem:

$$\begin{aligned} \min_{\lambda \in \mathfrak{L}} \quad & |\delta\mathbf{x}_{L,y}| \\ \text{s.t.} \quad & t_{min,i} \leq t_i \leq t_{max,i} \quad i = 1, ..., n \end{aligned} \tag{12}$$

Thus, as long as $dim(\mathfrak{L}) \geq 1$ (i.e. $n > 3$), it is possible to search for a set of cable tensions such that the displacement along a given direction is the smallest one.
There exist different methods to solve this problem: the Stiffness Oriented Tension Distribution Algorithm (SOTDA) developed in Picard et al. (2021) is the one used here.

4 Effect of the number of cables and their arrangement on the ACTS stiffness

This section attempts to quantify the influence of the number of cables and their arrangement on the stiffness of the ACTSs. However, since the arrangement and number of cables are coupled inside $\mathbf{K}$, it is necessary to develop a methodology that distinguishes their effects before being able to quantify them. Equation (5) can be rewritten as follows:

$$\begin{aligned} \mathbf{K} = & \sum_{i=1}^{3} k_i \mathbf{q}_i \mathbf{q}_i^T + \sum_{i=1}^{3} \frac{t_i}{l_i}(\mathbb{I}_3 - \mathbf{q}_i \mathbf{q}_i^T) \\ & + \sum_{j>3}^{n} k_j \sum_{i=1}^{3} a_{ij}^2 \mathbf{q}_i \mathbf{q}_i^T + \sum_{j>3}^{n} \frac{t_j}{l_j}(\mathbb{I}_3 - \sum_{i=1}^{3} a_{ij}^2 \mathbf{q}_i \mathbf{q}_i^T) \end{aligned} \tag{13}$$

where:

$$\mathbf{q}_j = \sum_{i=1}^{3} a_{ij}\mathbf{q}_i \qquad a_{ij} \in \mathbb{R},\, j = 4, \ldots, n \tag{14}$$

is expressed as linear combination of the vectors $\mathbf{q}_i$ which, in turn, generate the base $\mathfrak{B}_\ell$ (Lang, 2002):

$$\mathfrak{B}_\ell := \{\mathbf{q}_i \,|\, i = 1, 2, 3\} \qquad \ell = 1, \ldots, \infty \tag{15}$$

where subscript ℓ identify one base among infinity.

Table 2. ACTS parameters.

Symbols	Value	Symbols	Value
m	15 kg	$f_{min,i}$	150 N
l	2 m	$f_{max,i}$	450 N
d_{cable} (diameter)	0.7 mm	$\mathbf{w}_e$	$(0, \ -10, \ 0)^{\mathrm{T}}$ N
E_{cable} (Young modulus)	4 GPa		

Equation (13) provides some insight regarding the dependency of the matrix $\mathbf{K}$ on the system parameters described in Remarks 3.1. Assume that $k_1 = \cdots = k_n = k$, $l_1 = \cdots = l_n = l$ and that each cable direction and basis $\mathfrak{B}_\ell$ are randomly generated by using a *continuous uniform distribution* $\mathcal{U}$ (Weisstein, 1999). In particular, each component of $\mathbf{q}_i$ is generated as $\mathcal{U}([0,1])$. This makes the procedure general and systematic allowing each cable to take any direction in space. Hence, the variables that play an important role in the stiffness are, $\mathfrak{B}_\ell, a_{ij}, t_i, k, l$. Moreover:

- assign $\mathfrak{B}_\ell$ and assume $n > 3$, then according Behzadipour (2006):

$$\forall\, a_{ij} \in \mathbb{R} \ s.t. \ t_i > 0 \ \forall\, i \Rightarrow \mathbf{q}_i \mathbf{q}_i^T \geq 0 \ \Rightarrow \text{the larger } n, \text{the higher } k_{ds}$$

- assign $n \geq 3$ and assume the existence of a finite number of possible configurations: it becomes possible to estimate the mean $\tilde{k}_{ds}$ and standard deviation $\hat{k}_{ds}$ of k_{ds} as (Weisstein, 1999):

$$\tilde{k}_{ds} = \frac{k_{ds,max} + k_{ds,min}}{2} \tag{16}$$

$$\hat{k}_{ds} = \sqrt{\frac{(k_{ds,max} + k_{ds,min})^2}{12} \frac{n_c + 1}{n_c - 1}} \tag{17}$$

  where $k_{ds,max}$ and $k_{ds,min}$ represent the extreme values of the interval $\mathcal{I} = [k_{ds,min}, k_{ds,max}]$ to which k_{ds} belongs, whereas $\mathcal{I}$ is discretized into n_c elements.

To assess the effects of number of cables and cable arrangement, some parameters are set and given in Table 2. The directional stiffness index were computed $n_{eval} = 10^5$ times using the fixed set of data. Results are collected in Tables 3 and 4 and depicted in Figures 2. The mean value $\tilde{k}_{ds}$ is representative of the directional stiffness of all the configurations; independently from the cable arrangements. In parallel, the standard variation $\hat{k}_{ds}$, is an indicator of the influence of cable directions: it underlines the influence of changing $\mathfrak{B}_\ell$. These properties are inherent in the stiffness of the system modelled by

Table 3. 1^{st} Simulation data.

n	$\tilde{k}_{ds}$	$\hat{k}_{ds}$
3	304 N/m	1239 N/m
4	301 N/m	208 N/m
5	393 N/m	245 N/m
6	497 N/m	281 N/m
7	601 N/m	311 N/m
8	710 N/m	340 N/m
9	815 N/m	362 N/m
10	923 N/m	387 N/m

Table 4. 2^{nd} Simulation data.

n	$\tilde{k}_{ds}$	$\hat{k}_{ds}$
3	310 N/m	2436 N/m
4	301 N/m	204 N/m
5	395 N/m	245 N/m
6	499 N/m	282 N/m
7	602 N/m	311 N/m
8	708 N/m	338 N/m
9	813 N/m	363 N/m
10	924 N/m	386 N/m

equation (13): this is supported by the strong correlation between the results obtained from arbitrary simulations; as depicted in Figures 2.

Collected data shown that $\hat{k}_{ds}$ drop down rapidly in the transition between $n = 3$ and $n = 4$. Subsequent values of $\hat{k}_{ds}$ (from $n \geq 5$) decrease as the number of cables rises. Meanwhile, for $\tilde{k}_{ds}$, adding one cable leads to an increase in stiffness. In other words, the $\tilde{k}_{ds}$ variations due to a change of cable number become almost constant for $n \geq 5$.

Thus, from $n \geq 5$ the net difference between the effects of the number and direction of the cables on the stiffness becomes apparent.

These numerical results pave the way for a more general result:

Theorem 4.1. *Consider an ACTS with n cables and a point-mass end-effector. Then if $n \to \infty$, $\hat{k}_{ds}$ becomes constant.*

Proof. Let's pick two different bases $\mathfrak{B} := \{\mathbf{q}_i \,|\, i = 1, 2, 3\}$ and $\mathfrak{B}^* := \{\mathbf{q}_i^* \,|\, i = 1, 2, 3\}$ and assume that $k_1 = \cdots = k_\infty = k$, $l_1 = \cdots = l_\infty = l$.

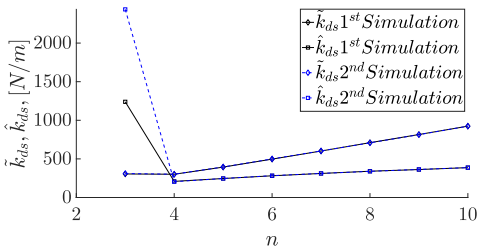

Figure 2. Directional stiffness (mean and standard deviation) as a function of the number of ACTS configurations.

It is straightforward to see that, given an external wrench $\mathbf{w}_e \in \mathbb{R}^3$, $\mathbf{t} = -\mathbf{W}^{\dagger}\mathbf{w}_e$ and $\mathbf{t}^* = -\mathbf{W}^{*\dagger}\mathbf{w}_e$ are equal because both $\mathbf{W}^{\dagger}$ and $\mathbf{W}^{*\dagger}$ contains all the direction vectors possible. Therefore, the new stiffness matrix $\mathbf{K}^*$ is:

$$\begin{aligned}\mathbf{K}^* = \sum_{i=1}^{3} k_i \mathbf{q}_i^* \mathbf{q}_i^{*T} + \sum_{i=1}^{3} \frac{t_i}{l_i}(\mathbb{I}_3 - \mathbf{q}_i^* \mathbf{q}_i^{*T}) + \sum_{j>3}^{n} k_j \sum_{i=1}^{3} a_{ij}^{*2} \mathbf{q}_i^* \mathbf{q}_i^{*T} \\ + \sum_{j>3}^{n} \frac{t_j}{l_j}(\mathbb{I}_3 - \sum_{i=1}^{3} a_{ij}^{*2} \mathbf{q}_i^* \mathbf{q}_i^{*T})\end{aligned} \tag{18}$$

with $a_{ij}^* \in \mathbb{R}$.
As before, using the concept of linear combination yields:

$$\mathbf{q}_i^* = \sum_{k=1}^{3} b_k \mathbf{q}_k \qquad b_k \in \mathbb{R},\ \mathbf{q}_k \in \mathfrak{B} \tag{19}$$

which substituted in (18), leads to:

$$\begin{aligned}\mathbf{K}^* = &\sum_{i=1}^{3} k_i \sum_{k=1}^{3} b_{ik} \mathbf{q}_k \mathbf{q}_k^T + \sum_{i=1}^{3} \frac{t_i}{l_i}(\mathbb{I}_3 - \sum_{k=1}^{3} b_{ik} \mathbf{q}_k \mathbf{q}_k^T) \\ &+ \sum_{j>3}^{n} k_j \sum_{i=1}^{3} a_{ij}^{*2} \sum_{k=1}^{3} b_{ik} \mathbf{q}_k \mathbf{q}_k^T + \sum_{j>3}^{n} \frac{t_j}{l_j}(\mathbb{I}_3 - \sum_{i=1}^{3} a_{ij}^{*2} \sum_{k=1}^{3} b_{ik} \mathbf{q}_k \mathbf{q}_k^T)\end{aligned} \tag{20}$$

with $b_{ik} \in \mathbb{R}$.

Subsequently, recalling that $\hat{k}_{ds} = f(\mathfrak{B}, a_{ij})$ and using the arbitrariness of the coefficients of the linear combination, gives us the results. □

Remark 4.2 (Numerical trend of $\Delta\hat{I}_{k_{ds}}$)**.** To shed light on Theorem 4 the trend of $\Delta\hat{I}_{k_{ds}} = \hat{I}_{k_{ds},s+1} - \hat{I}_{k_{ds},s}$ is depicted in Figure 3. Each step-s implies an increase of 10 cables in the configuration. It can be seen that as the number of cables n increases, $\Delta\hat{I}_{k_{ds}}$ decreases. Consequently when $n \to \infty$ then $\Delta\hat{I}_{k_{ds}} \to 0$ and $\hat{k}_{ds} = const.$

Corollary 4.3. *The arbitrariness of the coefficients of the linear combination leads to* $\mathbf{K} = \mathbf{K}^*$.

Proof. Once again, using equation (20), it is straightforward to see that there exists a set of coefficients for the linear combination (19) such that the two matrices $\mathbf{K} = \mathbf{K}^*$ are identical. □

Corollary 4.4. *The arbitrariness of the coefficients of the linear combination leads to* $\hat{k}_{ds} = \hat{k}^*_{ds}$.

Proof. Relying on Theorem 4, Corollary 4.3 and Remark 4.2, when $n \to \infty$ and $\Delta\hat{I}_{k_{ds}} \to 0$ then all the $\hat{k}_{ds}$ are constant and then equal one another $\hat{k}_{ds} = \hat{k}^*_{ds}$. □

Remark 4.5 (Empirical design rule)**.** The results of Corollary 4.4 involves design aspects of the ACTSs. It points out that for a high number of cables the effect of the configuration vanishes. Technically speaking, the limit on the number of cables can be set at 10. Indeed, Tables 2 and 3 show that by varying the number of cables in this range, $\Delta\hat{I}_{k_{ds}} \approx 20$ N/m $< \tilde{k}_{ds} \approx 100$ N/m.

In order to fully consider the influence of cable directions on stiffness, it is necessary to evaluate the lambda space $\mathfrak{L}$: it provides the possibility of picking a set of tensions that increases stiffness. The shape of $\mathfrak{L}$ and thus the tensions applicable to the cables depend on the configuration.

Hereby, we compare the directional stiffness of a classical ACTS with a hybrid one, both with $n = 5$. The classic ACTS is characterized by cables whose directions point upwards. In the hybrid, the 4th and 5th cables are attached to the ground as in Jamshidifar and Khajepour (2020), whereas the other three cables have the same directions as in the classical one shown in Figure 4.

In this example the directional stiffness index and the load-displacement $\delta\mathbf{x}_{L,y}$ are used for comparison. Figure 5 depicts the load-displacement within the available wrench set $\mathcal{W}$ for the classical and hybrid ACTSs.

In particular, the available wrench set is projected onto the cartesian planes and discretized, then the load-displacement $\delta\mathbf{x}_{L,y}$ is computed for all the points of the grid. The wrench sets generated are different for the two ACTSs: the relevant parameters that distinguish the two ACTS are summarized in Table

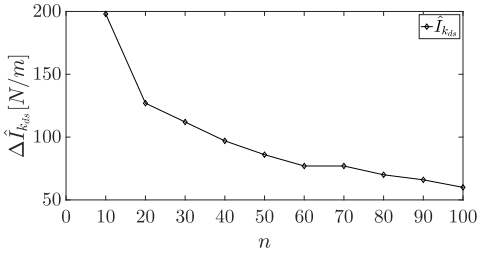

Figure 3. Decreasing trend of $\Delta\hat{I}_{k_{ds}}$ due to the increase in the number of cables.

Table 5. Features of classical and hybrid ACTS.

		$\mathcal{W}_{xy}$		$\mathcal{W}_{yz}$		$\mathcal{W}_{xz}$	
ACTS	Volume$_{\mathcal{W}}$	$\delta\mathbf{x}_{L,ymin}$	$\Delta\delta\mathbf{x}_{L,y}$	$\delta\mathbf{x}_{L,ymin}$	$\Delta\delta\mathbf{x}_{L,y}$	$\delta\mathbf{x}_{L,ymin}$	$\Delta\delta\mathbf{x}_{L,y}$
Classical	1.2 $e8$	0.021	0.0004	0.012	0.008	0.012	0.008
Hybrid	3.0 $e7$	0.018	0.005	0.018	0.006	0.018	0.004

$\Delta(\cdot)$ defines the difference between the maximum and the minimum $\delta\mathbf{x}_{L,y}$ values.

5. For the scope of this section, the important aspect of this analysis is that $k_{ds,Classical} = 467$ N/m and $k_{ds,Hybrid} = 470$ N/m are in accordance with the data collected in the Table 3 for $n = 5$. Indeed, the generated base $\mathfrak{B}$ is common for both the ACTS and the directional stiffnesses are similar between them and w.r.t. the mean value of $\tilde{k}_{ds}$ for $n = 5$. However, as the tensions depend on the configuration, the $\delta\mathbf{x}_{L,y}$ can be recomputed and eventually minimised using the SOTDA procedure. Figure 6 depicts the lambda space $\mathfrak{L}$ for the hybrid ACTSs only. Indeed, the lambda space $\mathfrak{L}$ of the classical ACTS degenerates in a point (i.e. $\boldsymbol{\lambda} = \mathbf{0}$). This crucial difference is due to the change in the cable arrangement. As a consequence, the proper choice of $\boldsymbol{\lambda}$ can guarantee a reduction of the displacement up to ≈ 2 times. Indeed, the new $k_{ds,Hybrid} = 1083$ N/m: it is higher than the maximum value gived in Table 3 because here the SOTDA is exploited.

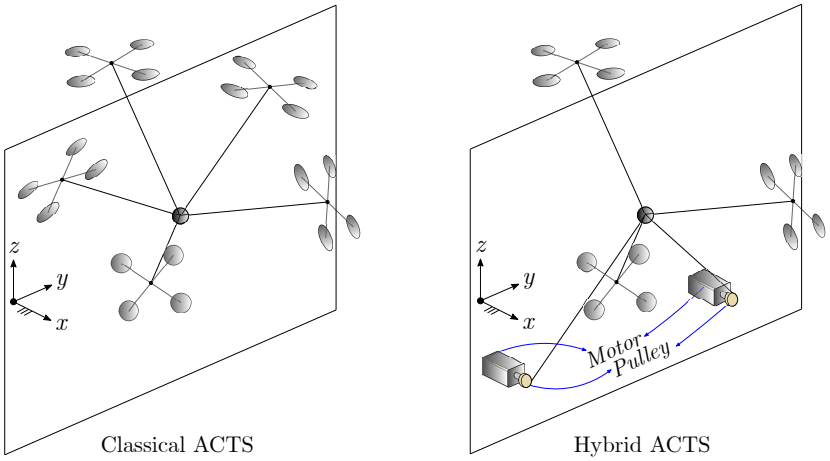

Figure 4. Classical and hybrid configurations of an ACTS with $n = 5$.

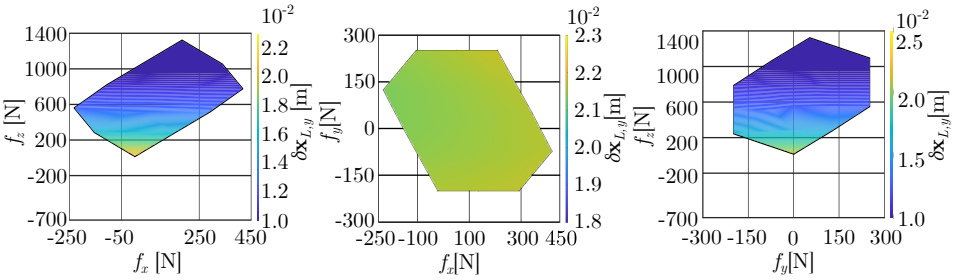

(a)

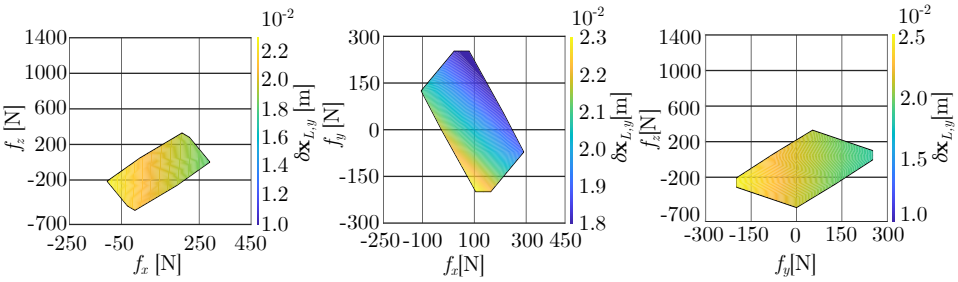

(b)

Figure 5. Estimated load-displacement $\delta \mathbf{x}_{L,y}$ within the 2D available wrench set for the classical (a) and hybrid (b) ACTS. The load is subjected to a wrench $\mathbf{w}_e = (0,\, -10,\, 0)^{\mathrm{T}}$ and its position is $\mathbf{x}_L = (0,\, 0,\, 1)^{\mathrm{T}}$.

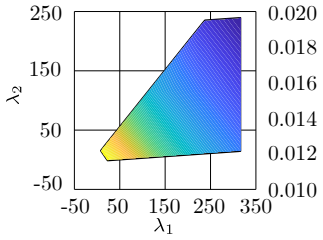

Figure 6. Estimated load-displacement $\delta \mathbf{x}_{L,y}$ over the lambda space $\mathfrak{L}$ for the hybrid ACTS.

5 Conclusion and future works

A preliminary study of the factors influencing the stiffness of ACTS was conducted in this paper. The results show that the cable arrangement of an ACTS

has a major impact on its stiffness. Indeed, the directional stiffness index is twice as important with the hybrid configuration of the ACTS than with the suspended configuration. Future work aims to generalize these results for systems with rigid body end-effector and to carry out the design of a controller capable of guiding the system to achieve the maximum index of directional stiffness. The theoretical results will be validated experimentally.

Bibliography

S. Behzadipour. Stiffness of cable-based parallel manipulators with application to stability analysis. *Journal of mechanical design*, 2006.

S. Bouchard, C. Gosselin, and B. Moore. On the ability of a cable-driven robot to generate a prescribed set of wrenches. *Journal of Mechanisms and Robotics, vol.2*, 2010.

J. Erskine, A. Chriette, and S. Caro. Wrench analysis of cable-suspended parallel robots actuated by quadrotor unmanned aerial vehicles. *Journal of Mechanisms and Robotics, vol. 11*, 2019a.

J. Erskine, A. Chriette, and S. Caro. Control and configuration planning of an aerial cable towed system. *Proceedings - IEEE International Conference on Robotics and Automation*, 2019b.

H. Jamshidifar and A. Khajepour. Static workspace optimization of aerial cable towed robots with land-fixed winches. *IEEE Transactions on Robotics, vol. 36*, 2020.

S. Lang. Algebra. *Springer Graduate Texts in Mathematics*, 2002.

A. Moradi. Stiffness analysis of cable-driven parallel robots. *Ph.D. thesis at Queen's University Kingston, Ontario, Canada*, 2013.

E. Picard, S. Caro, F. Plestan, and F. Claveau. Stiffness oriented tension distribution algorithm for cable-driven parallel robots. *Advances in Robot Kinematics 2020, vol. 15 Springer, Cham*, 2021.

A. L. C. Ruiz, S. Caro, P. Cardou, and F. Guay. Arachnis: Analysis of robots actuated by cables with handy and neat interface software. *2nd International Conference on Cable-Driven Parallel Robots*, 2015.

M. Tognon and A. Franchi. Theory and applications for control of aerial robots in physical interaction through tethers. *Springer Tracts in Advanced Robotics*, 2020.

D. K. D. Villa, A. S. Brandão, and M. Sarcinelli-Filho. Load transportation using quadrotors: A survey of experimental results. *International Conference on Unmanned Aircraft Systems (ICUAS)*, 2018.

C. Eric Weisstein. Discrete uniform distribution. *MathWorld, A Wolfram Web Resource*, 1999. URL `https://mathworld.wolfram.com/DiscreteUniformDistribution.html`.

L. Ya, Z. Fan, H. Panfeng, and Z. Xiaozhen. Analysis, planning and control for cooperative transportation of tethered multi-rotor uavs. *Aerospace Science and Technology, vol. 113*, 2021.